BRAIN CONNECTIVITY
Volume 11, Number 3, 2021

DOI: 10.1089/brain.2020.0808

Resting-State Functional Connectivity Disruption As a Pathological Biomarker in Autosomal Dominant Alzheimer Disease

Robert X. Smith,[1] Jeremy F. Strain,[1] Aaron Tanenbaum,[1] Anne M. Fagan,[1,2] Jason Hassenstab,[1] Eric McDade,[1] Suzanne E. Schindler,[1] Brian A. Gordon,[2,3] Chengjie Xiong,[4] Jasmeer Chhatwal,[5] Clifford Jack Jr.,[6] Celeste Karch,[2,7] Sarah Berman,[8] Jared R. Brosch,[9] James J. Lah,[10] Adam M. Brickman,[11] David M. Cash,[12] Nick C. Fox,[12] Neill R. Graff-Radford,[13] Johannes Levin,[14] James Noble,[11] David M. Holtzman,[1,2] Colin L. Masters,[15] Martin R. Farlow,[9] Christoph Laske,[16] Peter R. Schofield,[17] Daniel S. Marcus,[3] John C. Morris,[1,2] Tammie L.S. Benzinger,[2,3] Randall J. Bateman,[1,2] and Beau M. Ances,[1,2]; for the DIAN Network

Abstract

Aim: Identify a global resting-state functional connectivity (gFC) signature in mutation carriers (MC) from the Dominantly Inherited Alzheimer Network (DIAN). Assess the gFC with regard to amyloid (A), tau (T), and neurodegeneration (N) biomarkers, and estimated years to symptom onset (EYO).

Introduction: Cross-sectional measures were assessed in MC ($n = 171$) and mutation noncarrier (NC) ($n = 70$) participants. A functional connectivity (FC) matrix that encompassed multiple resting-state networks was computed for each participant.

Methods: A global FC was compiled as a single index indicating FC strength. The gFC signature was modeled as a nonlinear function of EYO. The gFC was linearly associated with other biomarkers used for assessing the AT(N) framework, including cerebrospinal fluid (CSF), positron emission tomography (PET) molecular biomarkers, and structural magnetic resonance imaging.

Results: The gFC was reduced in MC compared with NC participants. When MC participants were differentiated by clinical dementia rating (CDR), the gFC was significantly decreased in MC CDR >0 (demented) compared with either MC CDR 0 (cognitively normal) or NC participants. The gFC varied nonlinearly with EYO and initially decreased at EYO = −24 years, followed by a stable period followed by a further decline near EYO = 0 years. Irrespective of EYO, a lower gFC associated with values of amyloid PET, CSF Aβ_{1-42}, CSF p-tau, CSF t-tau, 18F-fluorodeoxyglucose, and hippocampal volume.

Conclusions: The gFC correlated with biomarkers used for defining the AT(N) framework. A biphasic change in the gFC suggested early changes associated with CSF amyloid and later changes associated with hippocampal volume.

Departments of [1]Neurology, [3]Radiology, and [4]Biostatistics, Washington University in Saint Louis, St. Louis, Missouri, USA.
[2]Hope Center for Neurological Disorders, Knight ADRC, Washington University, St. Louis, Missouri, USA.
[5]Department of Neurology, Massachusetts General Hospital, Boston, Massachusetts, USA.
[6]Department of Radiology, Mayo Clinic, Rochester, Minnesota, USA.
[7]Department of Psychiatry, Washington University School of Medicine, St. Louis, Missouri, USA.
[8]Department of Neurology, University of Pittsburgh, Pittsburgh, Pennsylvania, USA.
[9]Department of Neurology, Indiana University, Indianapolis, Indiana, USA.
[10]Department of Neurology, Emory University, Atlanta, Georgia, USA.
[11]Department of Neurology, Columbia University, New York, New York, USA.
[12]Department of Neurodegenerative Disease, Dementia Research Centre, Institute of Neurology, University College London, London, United Kingdom.
[13]Department of Neurology, Mayo Clinic, Jacksonville, Florida, USA.
[14]German Center for Neurodegenerative Disease (DZNE) Munich, Munich, Germany.
[15]The Florey Institute, University of Melbourne, Parkvile, Australia.
[16]Eberhard Karls University of Tubingen, Tubingen, Germany.
[17]Neuroscience Research Australia and School of Medical Sciences, The University of New South Wales (UNSW) Sydney, Sydney, Australia.

Keywords: amyloid; autosomal dominant Alzheimer disease; cerebrospinal fluid (CSF); estimated years to onset (EYO); 18F-fluorodeoxyglucose (FDG); hippocampus; positron emission tomography (PET); resting-state functional connectivity; tau

Impact Statement

This project focused on creating and evaluating a global functional connectivity (FC) signature that may serve as an outcome measure in clinical trials. This global FC signature encompassed multiple resting-state networks that included both inter- and intranetworks. Prior studies that focus on a single network may overlook important changes seen within and between networks. Our analysis is a logical progression from previous work that demonstrated that intra- and internetwork brain connections across multiple networks were affected with progression to cognitive impairment in autosomal dominant Alzheimer disease. This work revealed that FC disruption exhibits a nonlinear time course that was consistent with proposed biomarker models.

Introduction

Alzheimer disease (AD) is the leading cause of dementia in the United States. The occurrence of AD has been linked with β-amyloid (Aβ) peptide aggregating into plaques in the brain (Burdick et al., 1992). Aβ levels vary naturally following a circadian rhythm (Kang et al., 2009) and are associated with neuronal excitability (Palop et al., 2007). Excess production from neuronal hyperexcitability may underlie plaque formation (Mattsson et al., 2016; Palop et al., 2007). The amyloid cascade hypothesis (Mosconi., 2005) proposes that accumulation of Aβ plaques results in neurotoxic effects that are associated with tau accumulation and neurodegeneration culminating in cognitive dysfunction (as assessed by the clinical dementia rating [CDR]) (Bateman et al., 2012).

Autosomal dominant Alzheimer disease (ADAD) is caused by $\sim$100% penetrant mutations in genes that encode for the amyloid precursor protein (*APP*) (Bateman et al., 2011; Ryman et al., 2014; Schindler and Fagan, 2015) or gamma-secretase components, presenilin (*PSEN*) *1* and *PSEN2*. The ability to estimate when mutation-positive (mutation carriers [MC]) carriers will develop cognitive changes allows for modeling of disease based on estimated years to symptom onset (EYO). ADAD typically occurs at an earlier age compared with late-onset AD (LOAD) (Dubois et al., 2016; Frisoni, 2012; Smailagic et al., 2014) and is not associated with age-related comorbidities.

Pathologic changes start decades before clinical symptoms manifest in ADAD (Bateman et al., 2012). Recently, a set of biomarker criteria has been proposed to stage LOAD disease progression (Jack et al., 2012). This model describes that the earliest changes involve amyloid accumulation (A), followed by tau (T) deposition, and eventually neurodegeneration (N) that lead to cognitive dysfunction (Berti et al., 2010; Ewers et al., 2011; Fennema-Notestine et al., 2009; Frisoni et al., 2010; Klunk et al., 2004; Mosconi et al., 2010; Smailagic et al., 2015; Vlassenko et al., 2012).

Changes in amyloid biomarkers, such as cerebrospinal fluid (CSF) Aβ_{1-42} and Pittsburgh compound B (PiB) amyloid positron emission tomography (PET), have been observed $\sim$15–20 years before symptom onset in ADAD (Bateman et al., 2012; Berti et al., 2010; Brier et al., 2016; Forsberg et al., 2008; Gordon et al., 2018; McDade et al., 2018). Tau (T) biomarkers, such as CSF phosphorylated tau$_{181}$ (p-tau$_{181}$) (Schindler and Fagan, 2015), change $\sim$10–15 years before symptom onset in ADAD.

Neurodegeneration (N) biomarkers, such as CSF total tau (t-tau) (McDade et al., 2018; Schindler and Fagan, 2015) 18F-fluorodeoxyglucose (FDG) PET, a measure of glucose metabolism (Mosconi., 2005), and magnetic resonance imaging (MRI) measurements of hippocampal volume (Bateman et al., 2012; Bobinski et al., 2000; Gordon et al., 2018; McDade et al., 2018; Zarow et al., 2005), change at $\sim$5–10 years before EYO. CSF-based measures are sensitive to global levels of amyloid accumulation and tau deposition, but lack information pertaining to what brain regions are affected.

Imaging, on the contrary, provides spatially detailed information regarding impacted brain regions. In fact, PET imaging has revealed that amyloid may accumulate in a pattern of brain regions distributed across multiple functional brain networks (Thomas et al., 2014). This has led some to hypothesize that the pathological spread of disease through the brain occurs via brain networks (Forsberg et al., 2008; Thomas et al., 2014). However, a gap persists regarding when changes in brain networks occur with respect to AT(N) biomarkers in ADAD.

Resting-state functional connectivity (FC) noninvasively measures the association of signaling among brain regions and can be used to identify resting-state networks (RSNs) (Franzmeier et al., 2020). The inter-relationships among RSNs is sensitive to neuronal dysfunction and is associated with the degree of cognitive impairment (Frisoni et al., 2010; Frisoni., 2012; Frost and Diamond, 2010). A reduction in both intra- and internetwork FC occurs in ADAD (Gholipour et al., 2008). Global metrics of amyloid and tau accumulation aggregate spatially selective patterns for increased sensitivity. Similarly, a global FC signature can be derived from a combination of changes in intra- and internetworks that spans multiple RSNs (Power et al., 2012; Su et al., 2015). It remains important to know where changes in this global FC signature occur in the temporal progression of ADAD.

The purpose of this study is to evaluate the role of FC within the AT(N) framework in ADAD. Prior work has focused on select FC network differences, however, we use a data reduction strategy to compile information across multiple intra- and internetwork connections into a single global FC signature of ADAD. We assess FC strength based on a global FC signature between noncarriers (NC), MC asymptomatic (CDR 0), and MC symptomatic (CDR >0). We also evaluate the relationship between the global FC signature and established biomarkers that comprise the AT(N) framework and model the global FC signature as a function of EYO.

Methods

Participant characteristics

The cohort consisted of 171 individuals with ADAD mutations (MC) and 104 individuals from ADAD families who were genetically at-risk for inheriting the mutation but were not carriers (NC). All participants were enrolled in the international Dominantly Inherited Alzheimer Network (DIAN) and extracted from Data Freeze 11. Inclusion into this current analysis required that participants complete a general physical (including neurologic) examination, health and medication history, clinical assessment for dementia (Gordon et al., 2018), biochemical analysis, neuroimaging acquisition on only 3T Siemens Tim Trio scanners (Erlangen, Germany), and successful pass all quality control criteria (e.g., reduced motion during neuroimaging acquisition). All participants or their representatives provided written informed consent that was in accordance with the Washington University Institutional Review Boards or their respective institutions provided approval.

Clinical dementia rating

Experienced clinicians conducted semistructured interviews of each participant and a knowledgeable collateral source. The CDR was used to evaluate the degree of impairment (Morris, 1993). A score of CDR 0 indicates cognitively normal, CDR 0.5 corresponds to very mild dementia, and CDR ≥1 specifies mild to moderate dementia. Participants with a score of CDR >0 had a clinical diagnosis of AD dementia using previously described criteria (Greicius et al., 2003).

EYO estimation

Parent age at symptomatic onset was determined from semistructured interviews with the participant, a knowledgeable collateral source, and/or other informants familiar with the parental history of disease. The age at onset of the affected parent was determined by estimating the time of onset of consistent symptoms (e.g., memory/cognition, motor, or behavior) (Ryman et al., 2014). The EYO for each individual from DIAN was defined as age at testing minus the age at symptom onset for that individual's affected parent (Bateman et al., 2011).

Biochemical analyses

A lumbar puncture was performed in the morning under fasting conditions to obtain CSF using previously described methods (Bateman et al., 2012). Samples were shipped on dry ice to the DIAN biomarker core laboratory. CSF concentrations of $A\beta_{1-42}$, t-tau, and phosphorylated tau_{181} ($p\text{-}tau_{181}$) were measured by immunoassay (INNOTEST $A\beta_{1-42}$ and INNO-BIA AlzBio3, Innogenetics). All values met quality-control standards, including a coefficient of variation of 25% or less and kit ''controls'' that were within the expected range as defined by the manufacturer. Measurement consistency between plates of a common sample was included in each run.

Imaging

MRI data from only 3T Siemens Tim Trio scanners (Erlangen, Germany) were analyzed. Scanners were calibrated and used similar protocols. Structural images were acquired using the Alzheimer's Disease Neuroimaging Initiative (ADNI) protocol. T1-weighted scans were automatically segmented into regions of interest according to the Desikan atlas through FreeSurfer (Martinos Center for Biomedical Imaging, Charlestown, MA). Blood oxygen level-dependent (BOLD) FC was also acquired using previously described methods (Thomas et al., 2014). During the BOLD FC scans, participants were instructed to remain still with their eyes open and not fall asleep.

PET imaging was performed using FDG to measure glucose metabolism and PiB to measure amyloid load. PET imaging analyses were performed using a previously described PET Unified Pipeline (Su et al., 2013). Data from the 40- to 70-min postinjection window for PiB and 40- to 60-min window for FDG were converted to standardized uptake value ratios (SUVR) in the defined regions of interest using the cerebellar cortex as a reference region (Mintun et al., 2006). Partial volume correction was performed with a regional spread function (Su et al., 2015) that uses a geometric transfer matrix technique (Rousset et al., 2008). Global $A\beta$ was summarized as the average SUVR for the precuneus, lateral temporal, gyrus rectus, and prefrontal regions that have previously been shown to delineate AD from cognitively normal controls (Su et al., 2013). FDG from the precuneus was utilized as changes in this region are reliable and occur early in DIAN participants (Benzinger et al., 2013; Gordon et al., 2018; McDade et al., 2018).

FC preprocessing

BOLD FC preprocessing followed previously described methods (Brier et al., 2012, 2016; Thomas et al., 2014), including correction of odd versus even slice intensity differences attributable to interleaved acquisition and compensation for head movement within and across runs. Intensity inhomogeneity was corrected using FSL FAST (Zhang et al., 2001) followed by intensity normalization to obtain a whole-brain mode value of 1000. Echoplanar imaging (EPI) distortion due to magnetization inhomogeneity was corrected using a mean field map (Gholipour et al., 2008). Atlas transformation was computed by registering the EPI mean image to an atlas-representative template via the MP-RAGE (EPI → MP-RAGE → template). The template was generated from a separate cohort of 12 cognitively normal individuals. Compensation for head motion, distortion correction, and atlas transformation were sequentially combined to generate a volumetric time series that was resampled in $3mm^3$ atlas space.

Frames corrupted by excessive head motion were identified on the basis of both DVARS and frame displacement (FD) measures (Brier et al., 2014). In greater detail, the DVARS criterion was 0.9% root mean square of the frame-to-frame signal change from the entire brain (Afyouni Nichols, 2018; Power et al., 2012). The FD criterion was 0.3 mm. Frames were censored if either criterion was exceeded. The time series were band-pass filtered to retain frequencies between 0.005 and 0.1 Hz. For purposes of filtering, only a linear interpolation was applied over censored frames. Censored frames were excluded from all subsequent steps.

Denoising was accomplished using a CompCor-like strategy (Behzadi et al., 2007). In brief, nuisance regressors were

derived from three compartments (white matter, ventricles, and the extra-axial space) and then dimensionality reduced to create a matrix for singular value decomposition (SVD). White matter and ventricle masks were segmented in each individual using FreeSurfer 5.3 (Fischl, 2012) and spatially resampled to register with the FC data. Time series also were extracted from high-variance voxels (temporal standard deviation >2.5% relative to the whole-brain mode) in the extra-axial space (excluding the eyes). Nuisance regressors were derived from white matter, ventricles, and the extra-axial space. The final set of nuisance regressors included six parameters derived from rigid body head-motion correction, the global signal (GS) averaged over the (FreeSurfer-segmented) brain, and the GS temporal derivative. The preprocessed time series was nonlinearly warped to Montreal Neurological Institute (MNI) 152 space ($3\,mm^3$ voxels) space using FNIRT (Andersson et al., 2010; Jenkinson et al., 2002; Smith et al., 2004; Woolrich et al., 2009).

FC postprocessing

A putative set of 246 functional regions-of-interest (ROIs) were organized into 12 RSNs that included the sensorimotor (SM), sensorimotor-lateral (SMlat), cingulo-opercular (CO), auditory (AUD), ventral attention (VAN), visual (VIS), salience (SAL), default mode network (DMN), memory (MEM), dorsal attention (DAN), subcortical (SUB), and frontoparietal (FP) (Rousset et al., 2008). ROIs were defined as 10-mm-diameter spheres whose center coordinates were in MNI atlas space (Power et al., 2011). All ROIs were distinct and occupied unique voxels. A 246×246 FC matrix was obtained for each individual as follows. First, the preprocessed FC data were transformed on to the MNI atlas. Second, the mean time series was computed within each ROI excluding the censored frames. The pairwise correlation between all ROI time series was then derived. Correlation values were Fisher transformed for normality. The mean 246×246 FC matrix across all participants is shown in Figure 1 (left). We used each ROI's RSN designation (Power et al., 2011) to compute the average intra- and internetwork correlation reducing the FC to a 12×12 matrix. FC values along the diagonal blocks represent intra-RSN correlations, and values in the off diagonal blocks represent inter-RSN correlations. The mean 12×12 FC matrix across all participants is shown in Figure 1 (middle).

FC principal component analysis

Data reduction was performed to isolate a global FC signature metric of global FC changes (Smith et al., 2018; Su et al., 2015). The intra- and internetwork pattern of FC values from each participant was compiled, and a single global FC signature was selected. Specifically, the 12 intranetwork and $12 \times (12-1)/2 = 66$ internetwork averages (total of $12 + 66 = 78$) were compiled from all participants ($n = 275$) into a single 275×78 matrix. The principal component analysis (PCA) of this matrix was performed by SVD. PCA is a multivariate analysis that reveals internal data organization and its variance. This PCA revealed distinct FC patterns of intra- and internetwork averages across all RSNs. Each pattern comprised weights describing the influence from each

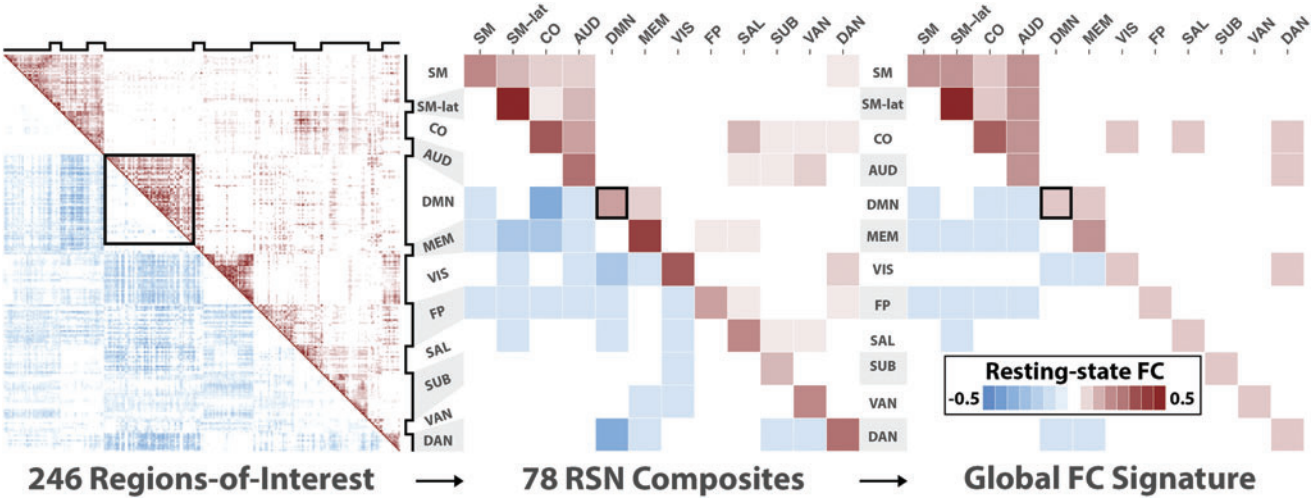

FIG. 1. PCA reveals a distributed pattern of FC changes across cortical and subcortical RSNs. Left: The mean FC matrix across all participants. An FC matrix from 248 regions of interest was computed for each participant. Positive correlations are shown in the upper triangle, and negatives are shown in the bottom triangle. Notched black lines on the top and to the right indicate RSNs. The black box outline is a visual aid highlighting the intranetwork FC values of the DMN. Middle: The mean FC-composite matrix across all participants. For each participant, an FC-composite matrix was generated by computing the mean intra- and internetwork FC matrix values (total of 78) for all 12 RSNs. Here the black box highlights the mean intranetwork FC value of the DMN. Right: The global FC signature is derived from the primary PCA pattern and reflects positively and negatively weighted mean FC-composite values. The strongest positive weights include the SM, SMlat, CO, AUD, VIS, and MEM. The strongest negative weights included the FP, MEM, DAN, and DMN. The black box outline highlights the weight of the mean intranetwork FC value of the DMN. AUD, auditory; CO, cingulo-opercular; DAN, dorsal attention; DMN, default mode network; FC, functional connectivity; FP, frontoparietal; MEM, memory; PCA, principal component analysis; RSNs, resting-state networks; SAL, salience; SM, sensorimotor; SMlat, sensorimotor-lateral; SUB, subcortical; VAN, ventral attention; VIS, visual. Color images are available online.

of the 78 intra- and internetwork FC composites on that pattern. The magnitude of a given weight reflects the strength of influence, while the sign, positive or negative, indicates whether the corresponding intra- or internetwork FC composite tends to increase or decrease, respectively, across participants. Each pattern was also accompanied by a set of scores that represented its association with each participant's pattern of FC values. The variability of these scores related to the total variability of FC values among participants. A low score indicates that the primary pattern is weakly present or absent from a participant. This implicates a strong deviation from, or decline in, the network connectivity specified by the primary pattern. The primary pattern that captured the largest percentage of total interindividual FC variance (21%) was designated the global FC signature for ADAD (Fig. 1, right). The same data reduction was applied to NC participants. The primary pattern from NC was very similar to the pattern computed for all participants, indicating that patient characteristics (abnormal levels of $A\beta_{42}$, tau, and neurodegeneration) are not strong factors in determining the primary pattern.

EYO modeling

Global FC signature versus RSN. We compared the abilities of the global FC signature and intranetwork values of the 12 RSNs included in this study to, separately, predict EYO using a leave-one-out cross-validation. Specifically, for each FC metric:

1. FC and EYO data were split into two sets: train and test. The training set comprised data from $N-1$ mutation-positive participants, and a test set comprised data from a single mutation-positive participant.
2. A linear predictive model was computed using the training set:

$$\mathrm{EYO}_{train} = \beta_0 + \beta_1 \mathrm{FC}_{train}$$

3. The linear model (i.e., coefficients β_0 and β_1) was used to predict EYO of the test set:

$$\mathrm{EYO}_{pred} = \beta_0 + \beta_1 \mathrm{FC}_{test}$$

4. The error in EYO was computed:

$$\mathrm{EYO}_{err} = \mathrm{EYO}_{test} - \mathrm{EYO}_{pred}$$

5. Steps 1–4 were repeated such that the FC data for each mutation-positive participant were used in the test set.
6. The sum of squares (SS) was computed for both $\mathrm{EYO}_{\mathrm{err}}$ and EYO:

$$\mathrm{SS}_{err} = \sum(\mathrm{EYO}_{err})^2$$

$$\mathrm{SS}_{EYO} = \sum(\mathrm{EYO})^2$$

7. The coefficient of determination (R^2), the proportion of the variance in actual EYO that is predictable from the FC, was computed:

$$R^2 = 1 - \frac{SS_{err}}{SS_{EYO}}$$

Nonlinear modeling. AD biomarkers exhibit nonlinear time courses across disease progression (Bateman et al., 2012; Jack et al., 2010; Kinnunen et al., 2018). Proposed biomarker models suggest nonlinear time courses with sigmoidal shape (Jack et al., 2010). The sigmoid transition time (i.e., when peak rate-of-change occurs) varies based on the biomarker. We investigated a sigmoidal shape of the global FC signature for MC participants to estimate transition times. An unweighted moving average of the global FC signature for MC participants was computed as a function of EYO using bin sizes of ±5 years to capture long-term trends. A model of staggered logistic decline evaluated the relationship between the global FC signature and EYO (t) for MC participants:

$$\text{global FC signature} = \mathrm{A}\left(\frac{1}{1+e^{-r(t-t_1)}} - \frac{1}{1+e^{-r(t-t_2)}}\right),$$

where A is carrying capacity, r is growth rate, and t_1 and t_2 are transition times. Here the carrying capacity describes the maximum FC that can be sustained. The growth rates and carrying capacities for both curves were constrained by goodness-of-fit using the Shapiro–Wilks test of normality on the residuals (Shapiro and Wilk, 1965). Nonlinear least-squares regression was performed using the ''nlm'' function in R (Dennis and Schnabel., 1983; R Core Team, 2017; Schnabel et al., 1985). The Akaike Information Criterion (AIC), Bayesian Information Criterion (BIC), and Levene's test were used to further evaluate model performance by comparing with polynomial models (i.e., linear, quadratic, and cubic) (Levene, 1960).

Association between global FC signature and AD biomarkers

Associations were computed between a participant's global FC signature and A/T/(N) biomarkers, including CSF biomarkers (log-transformed $A\beta_{1-42}$ [A1], p-tau_{181} [T1], and total-tau [N1]), PET molecular biomarkers (PiB mean cortical SUVR [A2] and FDG uptake in the precuneus [N2]), and a structural MRI biomarker (hippocampal volume [N3]). To investigate the relationship between global FC signature and AD biomarkers while adjusting for mediating associations, the partial correlation matrix (P) was computed by matrix inversion of the correlation matrix (R) such that the partial correlation between the i-th and j-th biomarkers was defined as follows:

$$p_{ij} = -\frac{s_{ij}}{\sqrt{s_{ii}s_{jj}}},$$

where s_{ij} were the elements of the inverted correlation matrix $S = R^{-1}$.

Results

Demographics

Cross-sectional FC data were obtained for NC ($n = 104$) and MC ($n = 171$) participants. NC individuals were older than MC CDR 0 ($p < 0.05$) participants, but younger than MC CDR >0 ($p < 0.05$) participants. Similarly, MC CDR 0 participants were younger than MC CDR >0 participants ($p < 0.05$) (Table 1).

Table 1. Demographic and Clinical Comparison of Non- and Mutation Carrier Groups

	NC	*MC*
n	104	171
Age: M (SD)	40.2 (11.3)	39.4 (11.3)
Gender (M/F)	41/63	74/97
CDR (0/0.5/ > 0.5)	104/0/0	99/46/26

CDR, clinical dementia rating; MC, mutation carrier; NC, noncarrier.

Spatial topology of the global FC signature of ADAD

We observed a global FC signature of ADAD, with strong contributions from both intra- and internetwork connections that spanned multiple RSNs (Fig. 1). This global FC signature was influenced by both positive and negative correlations and, for visual clarity, was separated along the diagonal based on the direction of influence on the global FC signature. Networks whose positive correlations had a strong influence included the SM, SMlat, CO, AUD, VIS, and MEM (intranetwork). Networks whose negative correlations had a strong negative influence included the FP, MEM (internetwork), DAN, and DMN.

The global FC signature associates with markers of disease progression

The global FC signature decreased with pathology. We observed that the global FC signature was significantly decreased in MC (yellow) compared with NC (gray) participants (Fig. 2A). When MC participants were further differentiated by CDR status, the global FC signature significantly decreased in MC CDR >0 (Fig. 2A, red; $p<0.05$) compared with either MC CDR 0 (green) or NC (gray) participants. NC and MC CDR 0 participants were not significantly different ($p>0.05$). For MC participants, a negative association was observed between mutation EYO and the global FC signature (Spearman's $\rho=-0.33$, $p=1.2e\text{-}05$; Fig. 2B). The association between the global FC signature and EYO remained significant after controlling for CDR status. We also observed that the global FC signature predicted, on average, 5 to 18 percent more variance for the actual EYO than internetwork RSN values (Fig. 2C).

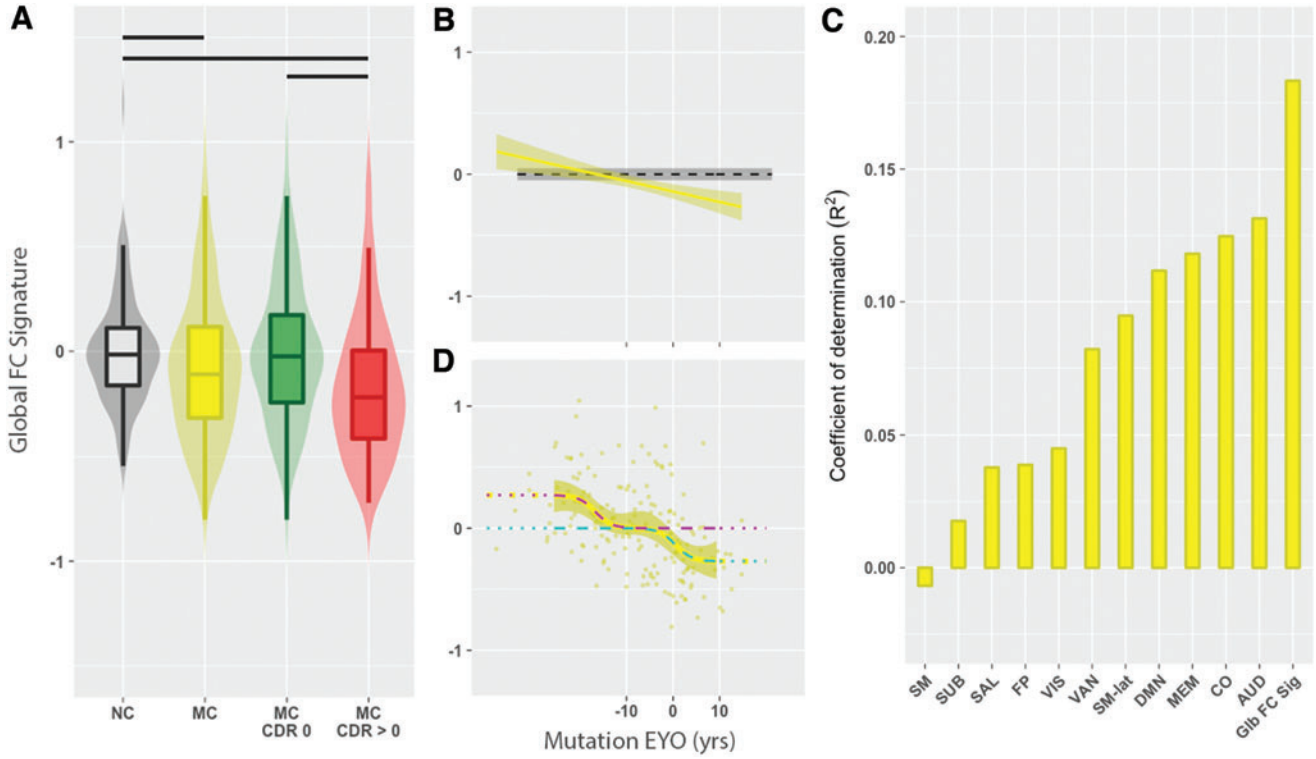

FIG. 2. **(A)** The global FC signature as a function of mutation status, CDR, and EYO. **(A)** Violin and box plots of the global FC signature for NC (gray) and MC (yellow), MC CDR 0 (green), and MC CDR >0 (red) participants. NC had a higher global FC signature compared with MC. MC CDR >0 had significant decreases in the global FC signature compared with NC and MC CDR 0 participants. A black bar represents a significant group difference. **(B)** Line plot showing the association between global FC signature and mutation EYO for MC participants. The global FC signature was associated with EYO in MC ($p<0.05$). The dashed line (black) is the mean global FC signature in NC participants, and the dark gray band is the confidence interval defined as two standard errors of the mean. **(C)** Coefficient of determination (R^2) for the global FC signature and the intranetwork values of 12 RSNs. The length of the vertical bar represents the strength of that FC value for predicting EYO. **(D)** The global FC signature for MC individuals exhibits a biphasic behavior with regard to mutation EYO in ±5-year bins. When the global FC signature was fit to the bin means (yellow curve), two logistic curves were observed (magenta and cyan). A two-stage process was observed, with early and late changes seen in the global FC signature. CDR, clinical dementia rating; EYO, expected years to symptom onset; MC, mutation carrier; NC, noncarrier. Color images are available online.

Nonlinear EYO modeling of the global FC signature

With regard to EYO, the global FC signature varied nonlinearly across the time course of the disease (Fig. 2D). This was consistent with a dual-logistic behavior model characterized by two transition times that were offset by ~ 17 years (Shapiro–Wilk's $W = 0.97$, $p = 0.28$). This nonlinear model (AIC = −161, BIC = −153) performed significantly better than the first-order (AIC = −128, BIC = −123), second-order (AIC = −128, BIC = −121), and third-order (AIC = −126, BIC = −118) polynomial models (Levene's $F = 4.04$, $p = 0.002$), and suggested a two-stage process. The global FC signature was elevated early in the disease time course (EYO < −16.7 years) in MC followed by a period that resembled control levels until further decreasing near the estimated time of symptom onset (EYO = 0.5 years).

Association between global FC signature and biomarkers

Strong associations were observed between CSF total tau and CSF p-tau$_{181}$ ($r = 0.86$, $p < 10E\text{-}16$), mean cortical PiB SUVR and CSF total tau ($r = 0.53$, $p = 1.7E\text{-}9$), mean cortical PiB SUVR and CSF p-tau$_{181}$ ($r = 0.65$, $p = 2.2E\text{-}16$), and precuneus PET FDG and hippocampal volume ($r = 0.53$, $p = 1.6E\text{-}09$).

Strong associations were observed between the global FC signature and several AD biomarkers (Fig. 3B, left). The global FC signature was compared with each AD biomarker classified according to the amyloid (A), tau (T), and neurodegeneration (N) framework (Fig. 3A). With regard to A criteria, the global FC signature was negatively associated with amyloid deposition as measured by mean cortical PiB SUVR ($p = 0.03$), and was positively correlated with CSF Aβ_{1-42} ($p = 0.007$). With regard to T criteria, the global FC signature was negatively associated with CSF p-tau$_{181}$ ($p = 0.009$). With regard to (N) criteria, the global FC signature was negatively associated with CSF total tau ($p = 0.02$), and positively associated with both precuneus PET FDG ($p = 0.002$) and hippocampal volume ($p = 0.001$). For each of these biomarkers, a worse global FC signature score was associated with greater pathology.

To investigate the strength of the direct pathological relationship between any two biomarkers (including the global FC signature), we controlled for potential mediating effects of general pathological decline. Specifically, an unbiased model was computed using a partial correlation matrix that controlled for other biomarkers (Fig. 3B, middle). In this unbiased model, no assumption of a specific temporal sequence of biomarkers was included. This network model strongly differentiated AT(N) biomarkers and agreed with previously hypothesized trajectories with amyloid measures strongly associating with each (A1 and A2), measure of tau (T1) strongly tied to neurodegeneration (N1), as well as measures of neurodegeneration group together (N1, N2, and N3) (Fig. 3B, right). In this model, the global FC signature most strongly associated with CSF Aβ_{1-42} (A1) and hippocampal volume (N3). These results provide further evidence of a two-stage process concerning the global FC signature with changes associating with early and late biomarkers. Moreover, these results suggest that each stage may be associated with changes in either amyloid accumulation or volumetrics.

Discussion

These results provide evidence that disruption of multiple functionally connected brain networks occurs in ADAD MC that is both stage dependent (asymptomatic versus symptomatic) and state dependent (biomarker status). Disruption of the global FC signature was greatest in symptomatic MC carriers. This indicates that changes in the global FC signature are tightly coupled with clinical presentation. However, even after adjusting for symptom severity using CDR, disruption of the global FC signature was significantly associated with disease progression, as measured by EYO. Furthermore, the global FC signature was, on average, a better predictor of EYO compared with intranetwork values of individual RSNs. Changes in the global FC signature were also associated with pathological biomarkers classified using the AT(N) framework for designating temporal progression of AD. Two independent methods showed that disruption of the global FC signature (1) occurred primarily during early (EYO ~ -17) and late (EYO ~ 0) stages, and (2) was associated with early-stage (CSF Aβ_{1-42}) and late-stage (hippocampal atrophy) biomarker changes. Taken together, these results suggest that the global FC signature may be sensitive to distinct processes affecting synaptic activity: Aβ accumulation early on in disease progression and neurodegeneration during later stages.

Our results are consistent with previous FC studies that investigated the disruption of specific RSNs in ADAD, but also shed new light on patterned changes across the entire spatial topography. Previous studies have primarily focused on FC changes within a single network. Changes have typically focused on the DMN, as this network has been associated with amyloid deposition (Buckner et al., 2009; Greicius et al., 2004) and is one of the largest networks with regard to the overall size in the brain (Greicius et al., 2003). In our current analysis, a global FC pattern of disruption was observed that included both intra and internetwork brain connections. These results suggest that prior studies primarily focusing on changes within a single network may overlook important changes seen within not only a network but also changes between networks. Our analysis is a logical progression from previous work that demonstrated that intra- and internetwork brain connections across multiple networks were affected with progression to cognitive impairment in ADAD (Thomas et al., 2014). In our current analysis, RSNs that associated with cognitive impairment included cognitive processing networks, including MEM, FP, DAN, and DMN, as well as sensory cortical regions such as the SM, SM-lat, VIS, and AUD. Cognitive processing regions that have been associated with the changes in pathological biomarkers, such as amyloid and tau accumulation and volume loss, and disruption of FC in these regions, may be associated with positivity of one or more biomarkers. Interestingly, neither FC nor pathological changes are typically observed in primary sensory regions. These results suggest that the FC disruption observed may be a precursor to subsequent pathology.

Disruption was greatest for symptomatic mutation carriers (MC CDR >0) compared with mutation NC. Our data showed that the greatest changes in the FC signature occurred for the symptomatic disease stage based on clinical

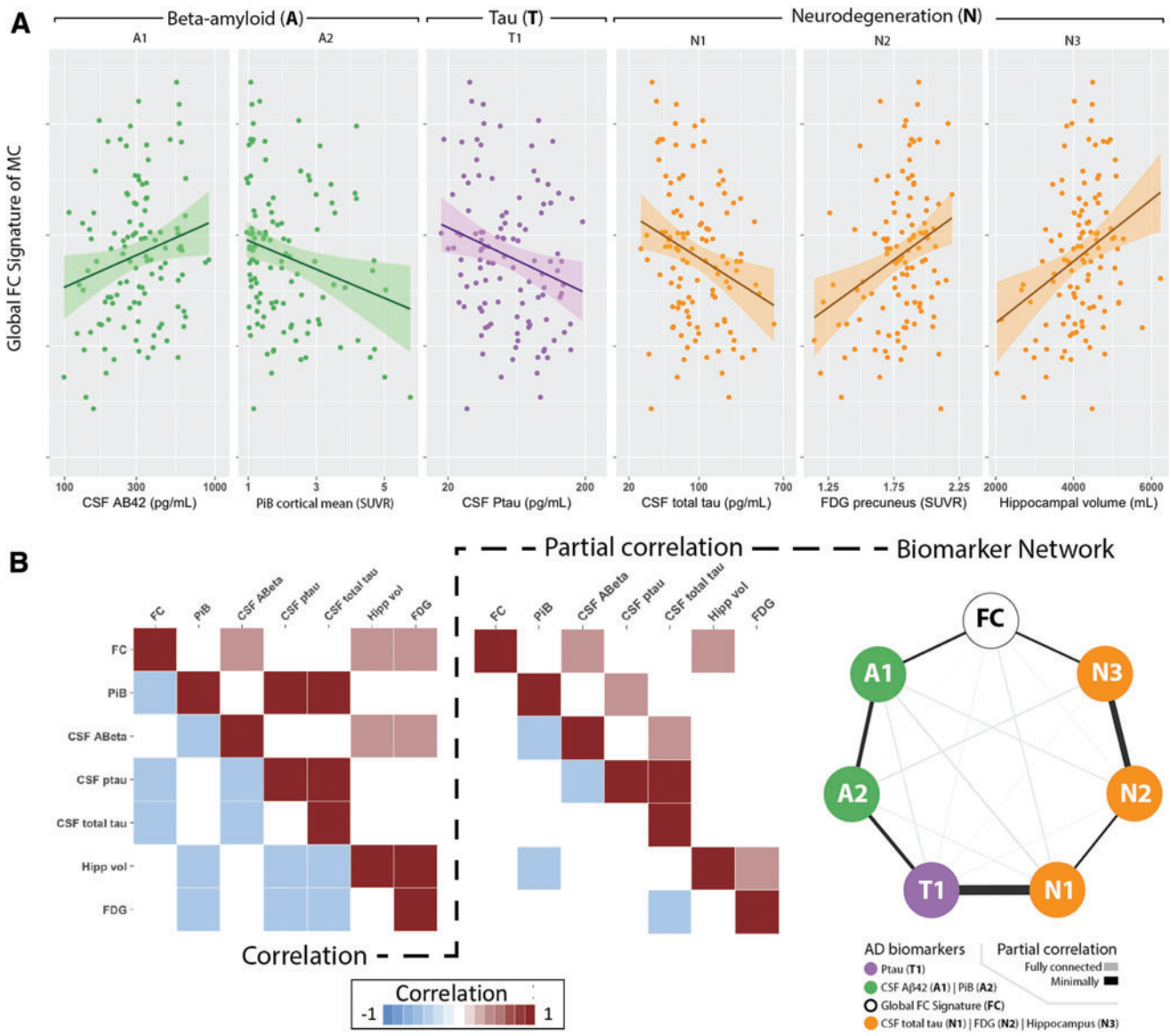

FIG. 3. The global FC signature as a function of Alzheimer disease (AD) biomarkers in mutation-positive (MC) individuals. Analyses investigated amyloid (A; green), Tau (T; purple), and neurodegenerative (N; orange) biomarkers. Scatter plots show that the global FC signature was **(A)** positively associated with CSF $A\beta_{1-42}$, negatively associated with mean PiB SUVR, negatively associated with CSF p-tau_{181} and total tau, and positively associated with both precuneus FDG uptake and hippocampal volume. **(B)** The correlation matrix of all biomarkers, including global FC signature (left), was inverted to compute the partial correlation matrix (middle). Network map of relationships was plotted among the global FC signature, and AD biomarkers based on the partial correlation matrix. The fully (light edges) and minimally (dark edges) connected graphs are shown. All associations were corrected for age. CSF, cerebrospinal fluid; FDG, 18F-fluorodeoxyglucose; PiB, Pittsburgh compound B; p-tau_{181}, phosphorylated tau_{181}; SUVR, standardized uptake value ratios. Color images are available online.

staging and genetic profile. Specifically, our data showed that 50% of the MC symptomatic cohort overlapped with the worst 25% of the asymptomatic MC cohort. This degree of overlap can be attributed to the classification scheme that is based on subjective responses during the clinical interview. This sensitivity to symptom manifestation bolsters the capability of this imaging marker as a tool for disease conversion. Future studies may assess the capability of an FC signature to redefine group classification to better identify individuals on the cusp of conversion.

Our results are consistent with previous FC studies that investigated disease progression using linear modeling, but also provide new insight regarding the time line of FC disruption. Linear modeling of disease progression suggests that FC disruption begins before the onset of symptoms. Consistent with previous results, we used a linear model and observed that FC disruption in certain RSNs occurred ~5 years before expected symptom inset (EYO −5) (Chhatwal et al., 2013). However, previous reports show that AD biomarkers exhibit nonlinear time courses across disease stages

(Dubois et al., 2016; Jack et al., 2010). In an updated model of disease progression, we observed that the global FC signature also exhibited a nonlinear time course that was consistent with proposed biomarker models (Jack et al., 2010). Specifically, disruption of the global FC signature was marked by two dramatic changes that occurred during very early ($\sim$17 EYO) and late ($\sim$0 EYO) disease stages in AD progression. The time period leading up to the initial decrease of the global FC signature could suggest a very early period of hyperconnectivity (Schultz et al., 2017). The production of Aβ has been linked to increased synaptic activity that can manifest as nonconvulsive seizures that are present before cognitive symptoms (Amatniek et al., 2006; Cirrito et al., 2005; Jack et al., 2010). FC hyperactivity has also been observed in LOAD particularly in areas with advanced Aβ accumulation (Ovsepian and O'Leary, 2016). It remains unclear whether this hyperactivity is detrimental due to synaptic excitotoxicity or compensatory due to increased pathological burden (Palop and Mucke, 2010). Our data suggest that this hyperactivity in FC may be a compensatory mechanism to preserve cognitive stability provided this observed state was years before symptom onset (Su et al., 2015). However, prolonged hyperactivity can lead to cognitive deficits and overall loss in connectivity strength (Thomas et al., 2014). This coincides with the second sharp decrease in the global FC signature that occurred at EYO = 0. This is consistent with evidence from MRI studies that show volume loss accelerates near EYO = 0 (Ewers et al., 2011). Together our data show an overall pattern that initiates with a decline from a hyperactive state that briefly returns to baseline levels before declining near symptom onset. These results suggest a dual-pathology process that reflects biological changes in the absence of behavioral changes. Understanding these distinct processes is clinically important for treatment intervention as individuals may respond differently based on their point on these curves.

The ability to characterize changes in a global FC signature during pre-clinical stages of AD was further supported by a separate linear model that focused on AT(N) biomarkers. A number of studies focusing on pathological biomarkers have proposed an AT(N) sequence in LOAD (Schnabel et al., 1985). Our model for ADAD was given no *a priori* assumptions concerning the sequence of biomarker events, except that the sequence should be consistent for participants. Despite our assumption of no specific temporal sequence of biomarker progression, our work further supports that ADAD and LOAD have similar temporal patterns for AD biomarkers regardless of the age of onset or genetic association (Schultz et al., 2017). Furthermore, we found that disruption of the global FC signature was preferentially associated with both CSF Aβ_{1-42} and hippocampal atrophy, biomarkers that characterize pathological changes occurring during the early and late stages of AD, respectively. This suggests that genetic mutations set in motion a time line of AT(N) biomarker changes with brain amyloidosis (possibly with certain soluble amyloid peptides proposed to be more closely associated with neuronal excitotoxicity) (A) followed by tauopathy (T) and eventually reduced glucose metabolism and brain volumetrics (N) (Bateman et al., 2011; Behzadi et al., 2007; Shapiro and Wilk, 1965).

Our results contribute to the understanding of how, in AD etiology, changes in global network functionality precipitate eventual short-term episodic memory deficits, the hallmark of AD. Based on these results it may be possible to use the global FC signature as a marker of underlying neuronal response to trials that introduce anti-Aβ therapies very early in the disease. Advantages for FC as an outcome measure in clinical trials include lack of radiation unlike PET biomarkers, and being less invasive than a lumbar puncture for CSF. Further studies should also look at changes in comparison with LOAD. Longitudinal studies of changes in FC in this cohort are needed to more robustly evaluate the nature of neuronal dysfunction with disease progression.

Acknowledgments

This article has been reviewed by the Dominantly Inherited Alzheimer's Network (DIAN) Study investigators for scientific content and consistency of data interpretation with previous DIAN Study publications. The authors acknowledge the altruism of the participants and their families and contributions of the DIAN research and support staff at each of the participating sites for this study. They thank Drs. Abraham Snyder and Mathew Brier for their helpful suggestions. They also thank all the participants for their involvement in the study and the DIAN sites for their recruitment and coordination of all studies.

Author Contribution

R.X.S.: Primary author of the article, developed the methodology, conducted the analyses, and contributed to the interpretation of the data. J.F.S.: Assisted in the conception and design of the study, consulted on the statistics, and reviewed the article. A.T. and A.M.F.: Assisted in the data analyses, statistics, and reviewed the article. J.H. and S.E.S.: Assisted in the data analyses and reviewed the article. E.M. and B.A.G.: Assisted in the original concept of the project, compiled the data, and reviewed the article. C.X.: Assisted in statistical analyses and reviewed the article. J.C., C.J. Jr., C.K., S.B., J.R.B., J.J.L., A.B., D.M.C., N.C.F., N.R.G.-R., J.L., J.N., D.M.H., C.L.M., M.R.F., C.L., P.R.S., D.S.M., J.C.M., T.L.S.B., R.J.B., and B.M.A.: Compiled the data and reviewed the article.

Author Disclosure Statement

R.X.S., J.F.S., A.T., A.M.F., J.H., S.E.S., C.X., J.C., C.K., S.B., J.J.L., A.B., D.M.C., J.L., J.N., C.L.M., C.L., and P.R.S.: Report no disclosures. E.M.: Research support: NIA, Eli Lilly, Roche, Janssen, GHR Foundation; Advisory Board: Eli Lilly; DSMB: Eli Lilly. B.A.G.: Involved in a clinical trial sponsored by Avid. C.J. Jr.: Consults for Eli Lilly, and serves on an independent data monitoring board for Roche but receives no personal compensation from and commercial entity. He receives research support from NIH/NIA and the Alexander Family Professor of Alzheimer's Disease Research, Mayo Clinic. J.R.B.: Research support includes AbbVie, Avanir, Biogen, Eisai, Eli Lilly, Genetech, Novartis, Roche, Suven Life Sciences Ltd. N.C.F.: Is on the scientific advisory board for Roche and Biogen. N.R.G.-R.: Research support includes AbbVie, Novartis, Biogen and Lilly. D.M.H.: Cofounded and is on the scientific advisory board of C2N diagnostics, LLC. Is on the scientific advisory board of Denali and consults for Genetech and AbbVie. M.R.F.: Research support includes AbbVie, Accera, ADCS, Posiphen, Biogen, Eisai, Eli Lilly, Genentech, Novartis, Suven Life Sciences, Ltd. He is on the advisory boards for

Accera, Allergan, Avanir, AZTherapies, Cognition Therapeutics, Cortexyme, Eli Lilly & Company, Longeveron, Green Valley, MedAvante, Merck and Co. Inc., Otsuka Pharmaceutical, Proclara, Neurotrope Bioscience, Regenera, Samumed, Takeda, vTv Therapeutics, Zhejiang Hisun Pharmaceuticals. D.S.M.: Funding support from Radiologics, Inc., and White-Rabbat.ai. J.C.M.: He is currently participating in clinical trials of antidementia drugs developed by Eli Lilly and Company, Biogen and Janssen. Dr. Morris serves as a consultant for Lilly USA. Research support from Eli Lilly/Avid Radiopharmaceuticals. T.L.S.B.: Involved in a clinical trial sponsored by Avid. R.J.B.: He is on the scientific advisory board for C2N Diagnostics. Research support from AbbVie, Biogen, Eisai, Eli Lilly, and Co/Avid Radiopharmaceuticals, Roche, Janssen, and United Neuroscience. B.M.A.: Involved in a clinical trial sponsored by Avid.

Funding Information

Data collection and sharing for this project were supported by the Dominantly Inherited Alzheimer's Network (DIAN, UF1AG032438) funded by the National Institute on Aging (NIA), the German Center for Neurodegenerative Diseases (DZNE), Raul Carrea Institute for Neurological Research (FLENI), partial support by the Research and Development, AMED, and the Korea Health Technology R&D Project through the Korea Health Industry Development Institute (KHIDI). Further support for this study was funded by NIH grants R01NR012907, R01NR012657, R01NR014449, P50AG05681, P01AG003991, P01AG026276, P30NS048056, UL1TR000448, R01AG04343404, R01AG052550, R01AG057680, K01AG053474, BrightFocus Foundation A2018817F, and NSF grant DMS1300280. Funding was also provided by the Charles F. and Joanne Knight Alzheimer's Research Initiative, the Hope Center for Neurological Disorders, and generous support from the Fred Simmons and Olga Mohan Fund, the Paula and Rodger O. Riney Fund, and the Daniel J Brennan MD Fund.

References

Amatniek JC, Hauser WA, DelCastillo-Castaneda C, et al. 2006. Incidence and predictors of seizures in patients with Alzheimer's disease. Epilepsia 47:867–872.

Andersson JLR, Jenkinson M, Smith S. 2010. Non-linear registration, aka spatial normalisation. FMRIB technical report TR07JA2. FMRIB Analysis Group of the University of Oxford 2:e21.

Afyouni S, Nichols TE. 2018. Insight and inference for DVARS. Neuroimage 172:291–312.

Bateman RJ, Aisen PS, De Strooper B, et al. 2011. Autosomal-dominant Alzheimer's disease: a review and proposal for the prevention of Alzheimer's disease. Alzheimers Res Ther 3:1.

Bateman RJ, Xiong C, Benzinger TL, et al. 2012. Clinical and biomarker changes in dominantly inherited Alzheimer's disease. N Engl J Med 367:795–804.

Behzadi Y, Restom K, Liau J, et al. 2007. A component based noise correction method (CompCor) for BOLD and perfusion based fMRI. Neuroimage 37:90–101.

Benzinger TLS, Blazey T, Jack CR, et al. 2013. Regional variability of imaging biomarkers in autosomal dominant Alzheimer's disease. Proc Natl Acad Sci U S A 110:e4502–e4509.

Berti V, Osorio RS, Mosconi L, et al. 2010. Early detection of Alzheimer's disease with PET imaging. Neurodegener Dis 7:131–135.

Brier MR, Gordon B, Friedrichsen K, et al. 2016. Tau and Abeta imaging, CSF measures, and cognition in Alzheimer's disease. Sci Transl Med 8:338ra66.

Brier MR, Thomas JB, Fagan AM, et al. 2014. Functional connectivity and graph theory in preclinical Alzheimer's disease. Neurobiol Aging 35:757–768.

Brier MR, Thomas JB, Snyder AZ, et al. 2012. Loss of intranetwork and internetwork resting state functional connections with Alzheimer's disease progression. J Neurosci 32:8890–8899.

Bobinski M, de Leon MJ, Wegiel J, et al. 2000. The histological validation of post mortem magnetic resonance imaging-determined hippocampal volume in Alzheimer's disease. Neuroscience 95:721–725.

Buckner RL, Sepulcre J, Talukdar T, et al. 2009. Cortical hubs revealed by intrinsic functional connectivity: mapping, assessment of stability, and relation to Alzheimer's disease. J Neurosci 29: 1860–1873.

Burdick D, Soreghan B, Kwon M, et al. 1992. Assembly and aggregation properties of synthetic Alzheimer's A4/beta amyloid peptide analogs. J Biol Chem 267:546–554.

Chhatwal JP, Schultz AP, Johnson K, et al. 2013. Impaired default network functional connectivity in autosomal dominant Alzheimer disease. Neurology 81:736–744.

Cirrito JR, May PC, O'Dell MA, et al. 2003. In vivo assessment of brain interstitial fluid with microdialysis reveals plaque-associated changes in amyloid-β metabolism and half-life. J Neurosci 23:8844–8853.

Dennis JE, Schnabel RB. 1983. *Numerical Methods for Unconstrained Optimization and Nonlinear Equations*. Englewood Cliffs, NJ: Prentice-Hall.

Dubois B, Hampel H, Feldman HH, et al. 2016. Preclinical Alzheimer's disease: definition, natural history, and diagnostic criteria. Alzheimers Dement 12:292–323.

Ewers M, Sperling RA, Klunk WE, et al. 2011. Neuroimaging markers for the prediction and early diagnosis of Alzheimer's disease dementia. Trends Neurosci 34:430–442.

Fennema-Notestine C, et al. 2009. Alzheimer's Disease Neuroimaging Initiative, Structural MRI biomarkers for preclinical and mild Alzheimer's disease. Hum Brain Mapp 30:3238–3253.

Fischl B. 2012. FreeSurfer. Neuroimage 62:774–781.

Forsberg A, Engler H, Almkvist O, et al. 2008. PET imaging of amyloid deposition in patients with mild cognitive impairment. Neurobiol Aging 29:1456–1465.

Franzmeier N, Koutsouleris N, Benzinger T, et al. 2020. Predicting sporadic Alzheimer's disease progression via inherited Alzheimer's disease-informed machine-learning. Alzheimers Dement 16: 501–511.

Frisoni GB. 2012. Alzheimer disease: biomarker trajectories across stages of Alzheimer disease. Nat Rev Neurol 8:299–300.

Frisoni GB, Fox NC, Jack CR Jr., et al. 2010. The clinical use of structural MRI in Alzheimer disease. Nat Rev Neurol 6:67–77.

Frost B, Diamond MI. 2010. Prion-like mechanisms in neurodegenerative diseases. Nat Rev Neurosci 11:155–159.

Gholipour A, Kehtarnavaz N, Gopinath K, . 2008. Average field map image template for Echo-Planar image analysis. Conf Proc IEEE Eng Med Biol Soc 2008:94–97.

Gordon BA, Blazey TM, Su Y, et al. 2018. Spatial patterns of neuroimaging biomarker change in individuals from families with autosomal dominant Alzheimer's disease: a longitudinal study. Lancet Neurol 17:241–250.

Greicius MD, Krasnow B, Reiss AL, et al. 2003. Functional connectivity in the resting brain: a network analysis of the default mode hypothesis. Proc Natl Acad Sci U S A 100: 253–258.

Greicius MD, Srivastava G, Reiss AL, et al. 2004. Default-mode network activity distinguishes Alzheimer's disease from healthy aging: evidence from functional MRI. Proc Natl Acad Sci U S A 101:4637–4642.

Jack CR, Knopman DS, Jagust WJ, et al. 2010. Hypothetical model of dynamic biomarkers of the Alzheimer's pathological cascade. Lancet Neurol 9:119–128.

Jack CR, Knopman DS, Weigand SD, et al. 2012. An operational approach to National Institute on Aging–Alzheimer's Association criteria for preclinical Alzheimer disease. Ann Neurol 71:765–775.

Jenkinson M, Bannister PR, Brady JM, et al. Improved optimisation for the robust and accurate linear registration and motion correction of brain images. Neuroimage 2002;17:825–841.

Kang J-E, Lim MM, Bateman RJ, et al. 2009. Amyloid-β dynamics are regulated by orexin and the sleep-wake cycle. Science 326:1005–1007.

Klunk WE, Engler H, Nordberg A, et al. 2004. Imaging brain amyloid in Alzheimer's disease with Pittsburgh Compound-B. Ann Neurol 55:306–319.

Kinnunen KM, Cash DM, Poole T, et al. 2018. Presymptomatic atrophy in autosomal dominant Alzheimer's disease: a serial magnetic resonance imaging study. Alzheimers Dement 14:43–53.

Levene H. 1960. Robust tests for equality of variances. In: Olkin I (ed.) *Contributions to Probability and Statistics: Essays in Honor of Harold Hotelling*. Standford, CA: Stanford University Press; pp. 278–292.

Mattsson N, Insel PS, Palmqvist S, et al. 2016. Increased amyloidogenic APP processing in APOE ε4-negative individuals with cerebral β-amyloidosis. Nat Commun 7:10918.

McDade E, Wang G, Gordon BA, et al. 2018. Longitudinal cognitive and biomarker changes in dominantly inherited Alzheimer disease. Neurology 91:e1295–e1306.

Mintun MA, Larossa GN, Sheline YI, et al. 2006. [11C]PIB in a nondemented population: potential antecedent marker of Alzheimer disease. Neurology 67:446–452.

Mosconi L. 2005. Brain glucose metabolism in the early and specific diagnosis of Alzheimer's disease. Eur J Nucl Med Mol Imaging 32:486.

Mosconi L, Berti V, Glodzik L, et al. 2010. Pre-clinical detection of Alzheimer's disease using FDG-PET, with or without amyloid imaging. J Alzheimers Dis 20:843–854.

Morris JC. 1993. The Clinical Dementia Rating (CDR): current version and scoring rules. Neurology 43:2412–2414.

Ovsepian SV, O'Leary VB. 2016. Neuronal activity and amyloid plaque pathology: an update. J Alzheimers Dis 49: 13–19.

Palop JJ, Chin J, Roberson ED, et al. 2007. Aberrant excitatory neuronal activity and compensatory remodeling of inhibitory hippocampal circuits in mouse models of Alzheimer's disease. Neuron 55:697–711.

Palop JJ, Mucke L. 2010. Amyloid-beta-induced neuronal dysfunction in Alzheimer's disease: from synapses toward neural networks. Nat Neurosci 13:812–818.

Power JD, Barnes KA, Snyder AZ, et al. 2012. Spurious but systematic correlations in functional connectivity MRI networks arise from subject motion. Neuroimage 59:2142–2154.

Power JD, Cohen AL, Nelson SM, et al. 2011. Functional network organization of the human brain. Neuron 72:665–678.

R Core Team. 2017. R: A language and environment for statistical computing. Vienna, Austria: R Foundation for Statistical Computing. https://www.R-project.org/ Last accessed March 24, 2021.

Rousset OG, Collins DL, Rahmim A, et al. 2008. Design and implementation of an automated partial volume correction in PET: application to dopamine receptor quantification in the normal human striatum. J Nucl Med 49:1097–1106.

Ryman DC, Acosta-Baena N, Aisen PS, et al. 2014. Symptom onset in autosomal dominant Alzheimer disease. Neurology 83:253–260.

Schindler SE, Fagan AM. 2015. Autosomal dominant Alzheimer disease: a unique resource to study CSF biomarker changes in preclinical AD. Front Neurol 6:142.

Schnabel RB, Koontz JE, Weiss BE. 1985. A modular system of algorithms for unconstrained minimization. ACM Trans Math Softw 11:419–440.

Schultz AP, Chhatwal JP, Hedden T, et al. 2017. Phases of hyperconnectivity and hypoconnectivity in the default mode and salience networks track with amyloid and tau in clinically normal individuals. J Neurosci 37:4323–4331.

Shapiro SS, Wilk MB. 1965. An analysis of variance test for normality (complete samples). Biometrika 52:591–611.

Smailagic N, Vacante M, Hyde C, et al. 2015. 18F-FDG PET for the early diagnosis of Alzheimer's disease dementia and other dementias in people with mild cognitive impairment (MCI). Cochrane Database Syst Rev 1:CD010632.

Smith RX, Jann K, Dapretto M, et al. 2018. Imbalance of functional connectivity and temporal entropy in resting-state networks in autism spectrum disorder: a machine learning approach. Front Neurosci 12:869.

Smith SM, Jenkinson M, Woolrich MW, et al. 2004. Advances in functional and structural MR image analysis and implementation as FSL. Neuroimage 23:208–219.

Su Y, D'Angelo GM, Vlassenko AG, et al. 2013. Quantitative analysis of PiB-PET with FreeSurfer ROIs. PLoS One 8:e73377.

Su Y, Blazey TM, Snyder AZ, et al. 2015. Partial volume correction in quantitative amyloid imaging. Neuroimage 107:55–64.

Thomas JB, Brier MR, Bateman RJ, et al. 2014. Functional connectivity in autosomal dominant and late-onset Alzheimer disease. JAMA Neurol 71:1111–1122.

Vlassenko AG, Benzinger TL, Morris JC. 2012. PET amyloid-beta imaging in preclinical Alzheimer's disease. Biochim Biophys Acta 1822:370–379.

Woolrich MW, Jbabdi S, Patenaude B, et al. 2009. Bayesian analysis of neuroimaging data in FSL. Neuroimage 45: S173–S186.

Zarow C, Vinters HV, Ellis WG, et al. 2005. Correlates of hippocampal neuron number in Alzheimer's disease and ischemic vascular dementia. Ann Neurol 57:896–903.

Address correspondence to:
Beau M. Ances
Department of Neurology
Washington University in Saint Louis
St. Louis, MO 63110
USA

E-mail: bances@wustl.edu